A&A 548, A55 (2012)
DOI: 10.1051/0004-6361/201220148

Astronomy & Astrophysics

Carbon and oxygen isotopic ratios in Arcturus and Aldebaran

Constraining the parameters for non-convective mixing on the red giant branch⋆

C. Abia[1], S. Palmerini[1], M. Busso[2], and S. Cristallo[3]

[1] Dpto. Física Teórica y del Cosmos, Universidad de Granada, 18071 Granada, Spain
e-mail: cabia@ugr.es
[2] Dipartimento di Fisica, Universitá di Perugia, and INFN, Sezione di Perugia, Italy
e-mail: [sara.palmerini;maurizio.busso]@fisica.unipg.it
[3] Osservatorio Astronomico di Collurania, INAF, 64100 Teramo, Italy
e-mail: cristallo@oa-teramo.inaf.it

Received 1 August 2012 / Accepted 27 September 2012

ABSTRACT

Context. We re-analyzed the carbon and oxygen isotopic ratios in the atmospheres of the two bright K giants Arcturus (α Boo) and Aldebaran (α Tau).

Aims. These stars are in the evolutionary stage following the first dredge-up (FDU). Previous determinations (dating back more than 20 years) of their $^{16}O/^{18}O$ ratios showed a rough agreement with FDU expectations; however, the estimated $^{16}O/^{17}O$ and $^{12}C/^{13}C$ ratios were lower than in the canonical predictions for red giants. Today these anomalies are interpreted as signs of the occurrence of non-convective mixing episodes. We therefore re-investigated this problem to verify whether the observed data can be reproduced in this scenario and if the fairly well determined properties of the two stars can help us in fixing the uncertain parameters that characterize non-convective mixing and in constraining its physical nature.

Methods. We used high-resolution infrared spectra from the literature to derive the $^{12}C/^{13}C$ and $^{16}O/^{17}O/^{18}O$ ratios from CO molecular lines near 5 μm, using the local termodynamic equilibrium (LTE) spectral synthesis method. We made use of the recently published ACE-FTS atlas of the infrared solar spectrum for constructing an updated atomic and molecular line lists in this spectral range. We also reconsidered the determination of the stellar parameters to build the proper atmospheric and evolutionary models.

Results. We found that both the C and the O isotopic ratios for the two stars considered actually disagree with pure FDU predictions. This reinforces the idea that non-convective transport episodes occurred in these stars. By reproducing the observed elemental and isotopic abundances with the help of parametric models for the coupled occurrence of nucleosynthesis and mass circulation, we derived constraints on the properties of non-convective mixing, providing information on the so far elusive physics of these phenomena. We find that very slow mixing, like that associated to diffusive processes, is incapable of explaining the observed data, which require a fast transport. Circulation mechanisms with speeds intermediate between those typical of diffusive and convective mixing are necessary. We conclude with a word of caution on the conclusions possible at this stage however, as the parameters for the mass transport are fairly sensitive to the stellar mass and initial composition. At least for α Boo, reducing the uncertainty still remaining on these data would be highly desirable.

Key words. stars: abundances – stars: individual: Arcturus – stars: individual: Aldebaran – stars: late-type

1. Introduction

Red giant branch (RGB) stars undergo evolutionary stages that start at the so-called first dredge-up (FDU), a convective mixing process that carries nuclei from internal layers to the surface, previously affected by CN cycling. The FDU occurs as the He-core contraction after the main sequence (MS) is accompanied by a downward envelope extension. It is now well established that this leads to a decrease in the $^{12}C/^{13}C$ ratio with respect to the MS value (~89 in the solar case), down to values in the range 15–30 (depending on the initial mass and metallicity of the star, see Weiss et al. 2000). In addition, the carbon abundance drops in the envelope, while that of nitrogen increases. If the stellar mass does not exceed ~2 $M_\odot$, the ^{16}O abundance remains unaltered, while that of ^{18}O is mildly reduced. The isotopic ratios $^{16}O/^{17}O/^{18}O$ expected by the models then lie on a characteristic line; their values depend on the initial stellar mass and have moved strongly in recent years as a consequence of changes in basic reaction rates (see for example Palmerini et al. 2011a, especially their Fig. 3). The present situation for these ratios as a function of the stellar mass, updated with the last version of the FRANEC evolutionary code (Cristallo et al. 2009, 2011) and with the last recommendations available for the relevant reaction rates (Adelberger et al. 2011) is summarized in Table 1.

Table 1. Oxygen isotopic ratios after FDU at solar metallicity.

Mass ($M_\odot$)	$^{16}O/^{17}O$	$^{16}O/^{18}O$
1	2571	526
1.2	2045	575
1.25	1784	587
1.3	1480	597
1.4	1095	613

This standard picture is challenged by a large amount of abundance determinations (see for example Brown & Wallerstein 1989; Gratton et al. 2000; Charbonnel 2004; Grundahl et al. 2002) in field- and globular cluster low-mass

⋆ Table 4 is available in electronic form at http://www.aanda.org

giant stars, showing very low $^{12}C/^{13}C$ ratios, sometimes almost reaching the equilibrium value of the CN cycle (~3.5). Anomalies in the C and O isotopes were found also in pre-solar C-rich and O-rich grains of stellar origin, preserved in meteorites (for example Amari et al. 2001; Nittler et al. 2008). In particular, Al_2O_3 grains reveal remarkable ^{18}O destruction (Nittler et al. 1997). Some families of this cosmic dust also display isotopic shifts in heavier elements including Mg and Al, and others have anomalies reaching up to neutron-capture elements beyond iron (for example Nicolussi et al. 1997, 1998).

Observationally, evidence of anomalies is often found in low-mass red giants ($\leq$2.3 $M_\odot$) for phases subsequent to the so-called *bump* of the luminosity function (BLF), when the advancing H-burning shell erases the chemical discontinuity left behind by the first dredge-up (Charbonnel & Balachandran 2000). This homogenization facilitates the occurrence of transport phenomena; hence, it became common to attribute the chemical anomalies to the occurrence of episodes of matter circulation in "conveyor belts" (Wasserburg et al. 1995; Nollett et al. 2003; Palmerini et al. 2011a) or in diffusive processes (Denissenkov et al. 1998; Eggleton et al. 2006). These phenomena (known under the names of *deep mixing*, *extra-mixing*, or *cool bottom processes*) would link the envelope to regions where proton captures take place, thus accounting for the observation that the photospheric material has undergone extensive processing.

Among the proposed physical causes for mixing mechanisms one can mention rotation itself through shear effects (Zahn 1992; Weiss et al. 2000; Charbonnel 2004) and meridional circulation (Talon 2005); gravity waves (Denissenkov & Tout 2003); magnetic buoyancy (Busso et al. 2007; Denissenkov et al. 2009); and molecular weight inversions leading to heavier materials falling down in a lighter environment (Eggleton et al. 2006). This last process was identified by Charbonnel & Zahn (2007) as the known thermohaline double-diffusion also occurring in the oceans which was previously studied by Ulrich (1971) in astrophysical environments.

Although all these physical phenomena may have a role in the complex dynamics that link red giant envelopes to their underlying radiative layers, it is not clear today in which evolutionary stage each of them works more efficiently (Uttenthaler et al. 2007), which range of stellar masses is affected and, therefore, which of them is more suited to explain the abundance changes in RGB stars. Even the requirement that the mixing episodes occur after the BLF has recently been questioned (Drake et al. 2011).

In general, the mentioned elusive processes are not treated in canonical stellar models; in some cases they are intrinsically linked to the stellar rotation or to the development of dynamical instabilities, thus requiring at least two-dimensional hydro-codes to be properly modeled. However, the use of 2D schemes for general stellar evolution is in its infancy (at best).

One has also to notice that clarifying the physics that is behind the chemical peculiarities is made difficult because the interpretation of observations is usually hampered by uncertainties in fundamental parameters of the chosen stars (stellar mass, luminosity, etc.). The sources we consider in this paper, Arcturus (α Boo) and Aldebaran (α Tau), are K-type RGB stars of nearly solar mass; they are very bright, are situated at a precisely known distance from the Sun and are well observed. Therefore, they may be less affected than others from this last difficulty, and can be considered as good references for studying stellar evolution and spectroscopic abundances in first-ascent red giants. Indeed, the determination of their observed parameters (luminosity, radius and effective temperature) is quite reliable and their high brightness facilitates the task of obtaining high-resolution, high signal-to-noise-ratio (S/N) spectra. This is so for both optical and infrared wavelengths, which allows an accurate abundance analysis.

It has been known for decades that the $^{12}C/^{13}C$ ratios of α Boo and α Tau share the problems discussed above for common red giants, being lower than predicted by the FDU. Hinkle et al. (1976) and Tomkin & Lambert (1984) early derived ratios of 7 and 12 for these stars, for Arcturus and Aldebaran. These first estimates were then confirmed by subsequent works (see for example Smith & Lambert 1990; Peterson et al. 1993). Thus, the anomaly in their C isotopic ratios is a quite robust result[1].

On the other hand, a previous determination of the oxygen isotopic ratios in these stars (Harris & Lambert 1984), using CO lines at 2 and 5 μm, indicated $^{16}O/^{17}O \sim 1100$, $^{16}O/^{18}O \sim 550$ for Arcturus, and $^{16}O/^{17}O \sim 660$, $^{16}O/^{18}O \sim 475$ for Aldebaran. The uncertainty was about 40–50%[2]. Harris & Lambert noticed the difficulty of simultaneously explaining the $^{12}C/^{13}C$ and $^{16}O/^{17}O$ ratios in these stars within the framework of the canonical FDU models. They proposed several possible solutions: among others, strong mass loss prior to the FDU, slow mixing during the main sequence and/or a reduction in the rate for $^{18}O(p, \alpha)^{15}N$. No satisfactory solution was found however, therefore the problem remained open since then.

Recent theoretical calculations at solar metallicity (Palmerini et al. 2011a), including revisions of critical nuclear rates[3], for masses close to 1.2 $M_\odot$, found O isotopic ratios shown in Table 1[4]. A quick inspection of Table 1 reveals that, considering the observational uncertainty in the Harris & Lambert data for oxygen, the $^{16}O/^{18}O$ ratios in both stars can be considered to roughly agree with the new theoretical predictions of stars with ~1.2 $M_\odot$, but clearly this is not the case for the $^{16}O/^{17}O$ ratio. The purpose of this work is to try to solve this problem, possibly also deriving additional hints on the extra-mixing parameters that physical models must reproduce.

In Sect. 2 we summarize the input data for our analysis, namely the spectra we used, the stellar parameters, and the chemical analysis tools we adopted. Section 3 is then devoted to the description of the non-convective models assumed for explaining the newly determined C and O isotopic ratios of our two program stars. In Sect. 4 we then comment on the values found for the extra-mixing parameters and we derive some general conclusions on this basis.

2. Input data

2.1. Observed data and line lists

For Arcturus we used the electronic version of the Infrared Atlas Spectrum by Hinkle et al. (1995). We analyzed the ~5 μm-region

[1] The derivation of this ratio, mainly from optical bands (CN lines in the region ~8000 Å) and from the infrared domain (CO lines at ~2.3 μm), is fairly insensitive to the adopted stellar parameters. Indeed, these parameters affect the $^{12,13}CN$ and/or $^{12,13}CO$ lines almost equally.

[2] We report here only the O ratios derived by the above authors from the 5 μm region, as in the 2 μm region the available CO lines for K giants are usually weak and blended.

[3] Among which the new measurement of $^{18}O(p, \alpha)^{15}N$ cross section provided by La Cognata et al. (2010).

[4] These predictions do not change significantly with metallicity in the range $-0.5 \leq$ [Fe/H] ≤ 0.0. (In the present work, we adopt the standard notation [X/H] = $\log(X/H)_\star - \log(X/H)_\odot$ where (X/H) is the abundance of the element X by number in the scale log (H) $\equiv$ 12.)

spectra rationed to the telluric spectrum. Accurate wavelength positioning and identification of the main species contributing in this region were recently performed in the solar infrared spectrum by Hase et al. (2010). In particular, in the range 1800–2200 cm^{-1} there are many weak and unblended $^{12}C^{17}O$ and $^{12}C^{18}O$ lines that are very sensitive to changes of the O isotopic ratios. For Aldebaran, we used a spectrum in a similar but shorter spectral region obtained on February 6, 1980 at the KPNO 4 m coudé telescope using a Fourier transform spectrometer. This spectrum was kindly provided by Hinkle. It has a spectral resolution of 0.016 cm^{-1}, slightly lower than that of Arcturus (0.01 cm^{-1}). The spectrum of Aldebaran was cleaned from telluric absorptions using the telluric spectrum of Arcturus (after some spectral resolution degradation) with the IRAF task *telluric*. At the wave number position of the strongest telluric absorptions the removal was, however, unsatisfactory, thus these spectral regions were excluded from the analysis. A difficulty in this procedure is that many peaks are found above the level of unity in the rationed spectra. We detected these highest peaks (excluding those close to the regions with the strongest telluric absorptions) and fited a smooth curve passing through them following the similar method used by Tsuji (2009) in Arcturus to place the continuum level in the rationed spectra. It is uncertain whether the continuum adopted in this way is a true continuum; however, different fits to these peaks resulted in very small differences (≤1%) in the continuum level.

We made use of an improved molecular line lists in the ∼5 μm region. Our list includes the molecules CO, C_2, CN, OH, SiO, MgH, SiS, and H_2O, of which CO is the main contributing molecule in the spectral region. CO lines were taken from Goorvitch (1994); C_2 lines are an update of Querci et al. (1971, priv. comm.); CN lines were taken from Plez (priv. comm.) as an update after the new energy levels calculated by Ram et al. (2010a,b); H_2O lines were taken from Barber et al. (2006); SiO lines were taken from Langhoff & Bauschlicher (1993); MgH lines were taken from Skory et al. (2003); OH were taken from Goldman et al. (1998), SiS were taken from Cami et al. (2009) and OH ones from the HITRAN database (Rothman & Gordon 2009). The atomic lines were taken from the VALD v-0.4.4 database (Kupka et al. 2000). A few line positions and intensities (mainly CO lines) were corrected by comparing a theoretical spectrum of the Sun with the infrared solar spectrum (Hase et al. 2010). We used a MARCS atmosphere model for the Sun (Gustafsson et al. 2008) with the solar abundances set from Asplund et al. (2009). For the C and O isotopic ratios in the Sun we also adopted the values suggested by these authors. The fit to the solar spectrum was excellent, in particular between 2100–2200 cm^{-1} where most of the $^{13}C^{16}O$, $^{12}C^{17,18}O$ lines used to derive the C and O ratios were selected.

2.2. Atmosphere parameters

α Tau and α Boo have been extensively studied with high-resolution, high-S/N spectra since 1980. Their atmospheric parameters have been estimated by several authors using a variety of techniques. For Arcturus, the simple mean and standard deviation for the stellar parameters compiled in the PASTEL database (Soubiran et al. 2010) is $T_{\rm eff}$ = 4324 ± 90 K, $\log g$ = 1.71 ± 0.29, and [Fe/H] = −0.56 ± 0.1, while for Aldebaran is $T_{\rm eff}$ = 3850 ± 40 K, $\log g$ = 1.2 ± 0.4, and [Fe/H] = −0.16 ± 0.1. Despite the considerable number of studies on these stars, the published parameters still do distribute randomly around the mean values, because of systematic errors, which vary among different studies[5]. We decided, therefore, to adopt the most recent determinations of the atmospheric parameters for these two stars. These are based on high-quality visual and infrared spectra and the use of MARCS model atmospheres (the same grid that we use here). For Arcturus we adopted the parameters derived in Ryde et al. (2009) and for Aldebaran those from Ramírez et al. (2009) and Alves-Brito et al. (2010, see Table 2). The adopted values, in any case, do not differ significantly from the average values given in the PASTEL database. In the references quoted above the C, N, and O, abundances were derived, as well as those for other species that are important for the opacity of the model atmospheres (Si, Ca, Mg, S, Ti, etc. see the original works for details). However, the atomic features present in the 5 μm region in both stars are very weak or severely blended; therefore we adopted the elemental abundances given by the authors except for the CNO elements. Variations up to ±0.25 dex in the metallicity of the stars have no impact on the derived C and O isotopic ratios.

Table 2. Stellar parameters used to derive CNO abundances and isotopic compositions in α Boo and α Tau.

	α Boo	α Tau	Ref.
Name	Arcturus	Aldebaran	
HR	5340	1457	
MK type	K1.5 III	K5 III	
$T_{\rm eff}$ [K]	4290 ± 50	3981 ± 75	a
L [$L_\odot$]	196 ± 21	440 ± 20	b
$\log(g$ [cm s^{-2}])	1.50 ± 0.10	1.20 ± 0.30	a
R [$R_\odot$]	25.4 ± 0.2	45.2 ± 0.7	a
[Fe/H]	−0.50 ± 0.07	−0.13 ± 0.13	a
$\xi_{\rm micro}$ [km s^{-1}]	1.7±0.1	1.94 ± 0.20	a
M [$M_\odot$]	1.08 ± 0.06	1.3 ± 0.3	b

Notes. The following references are for Arcturus and Aldebaran in the same order: [(a)] Ryde et al. (2009); Ramírez et al. (2009) and Alves-Brito et al. (2010). [(b)] Ramírez & Allende Prieto (2011); Lebzelter et al. (2012, and references therein).

A spherical MARCS model atmosphere (Gustafsson et al. 2008) was interpolated for each star from the grid of models for the parameters: $T_{\rm eff}$, $\log g$, [Fe/H], $\xi_{\rm micro}$ (see Table 2). We assumed for both stars 1 $M_\odot$ and for Arcturus we adopted an α-enhanced model ([α/Fe] = +0.4) as suited to its metallicity (Peterson et al. 1993). We note that Arcturus has a chromosphere (for example Ayres & Linsky 1975), therefore the continuum flux is enhanced at wavelengths shorter than about 2000 Å. This flux excess might be explained using a binary model (Verhoelst et al. 2005), but in this study we considered Arcturus as a single star because the impact of the possible secondary companion is only important in the ultraviolet, a region that we did not use and that therefore does not affect our analysis.

2.3. Analysis of the C and O ratios

For each of the model atmospheres, synthetic LTE spectra were calculated in the region 1850–2200 cm^{-1} with a step of 0.0002 cm^{-1} using the TURBOSPECTRUM v9.02 code described in Alvarez & Plez (1998) and the line list given above. The theoretical spectra were convolved with a Gaussian function with a *FWHM* ∼ 600–800 mÅ to mimic the spectral

[5] A recent discussion on the current techniques to derive atmospheric parameters and the associated errors can be found in Lebzelter et al. (2012).

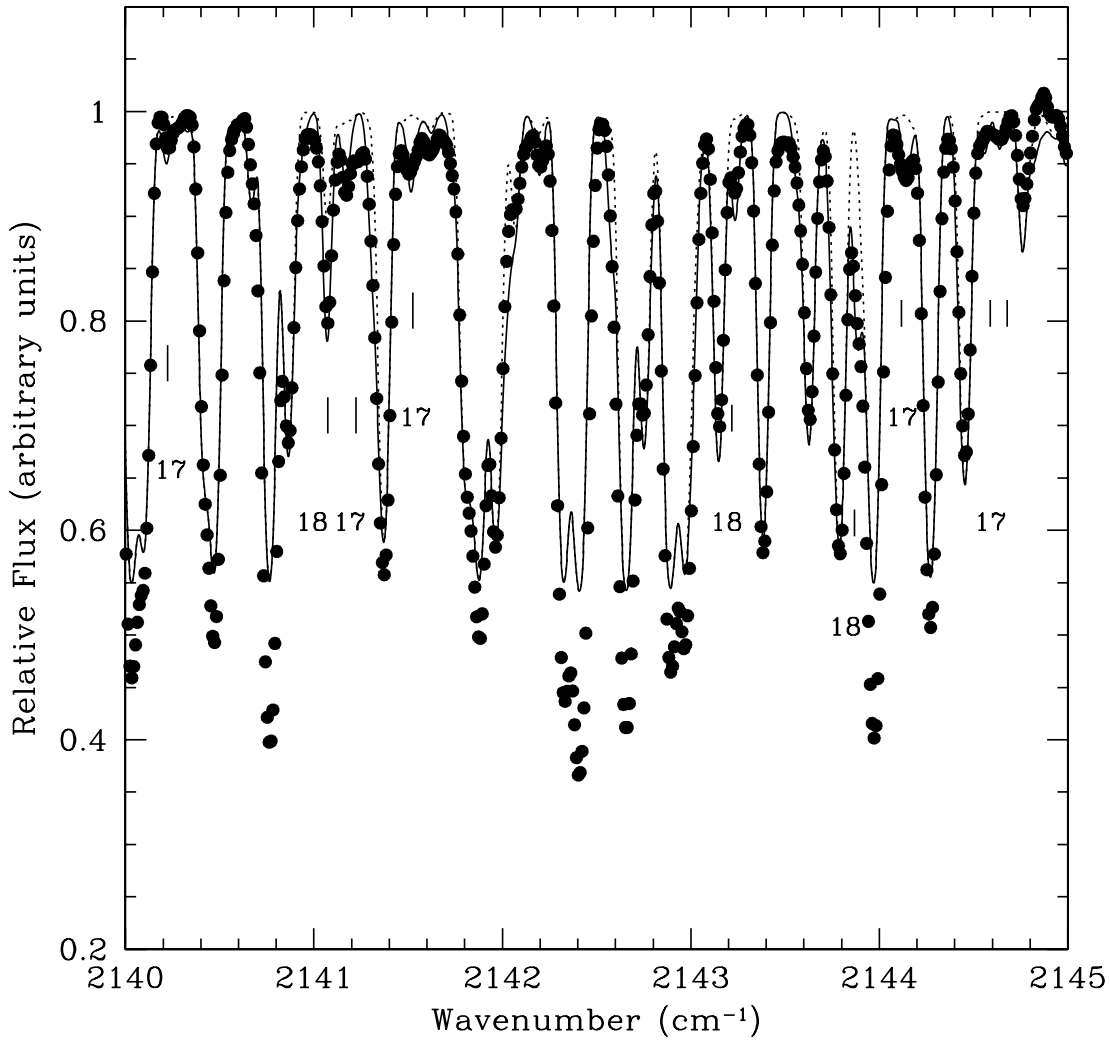

Fig. 1. Comparison of observed (dots) and synthesized spectra (lines) of Arcturus for different O ratios. Dotted line: $^{12}C/^{13}C$ = 9 and $^{17}O/^{16}O = {}^{18}O/^{16}O = 0$; continuos line: the same $^{12}C/^{13}C$ with $^{17}O/^{16}O$ = 3030, $^{18}O/^{16}O$ = 1660. Note that the cores of the more intense CO lines are not reproduced by the theoretical spectrum (see text). Some of the $C^{17}O$ and $C^{18}O$ lines used are marked.

resolution plus the macroturbulence parameter. To estimate the C abundance and the $^{12}C/^{13}C$ ratio, we selected a number of $^{12,13}CO$ lines that are weak, unblended and, apparently, not affected by the procedure for removing telluric absorption. We note that variations in the N abundance by ∼±0.3 dex have no effect on the synthetic spectrum. Moroever, the $^{12}C^{16}O$ lines are not very sensitive to changes to the O abundance by ∼±0.2 dex, thus we decided to adopt in our stars the N and O abundances derived by Ryde et al. (2009) and Ramírez et al. (2009)[6]. It is important to note that in selectioning these CO lines we took into account the fundamental problem of the 5 μm spectrum of K giants (for example Heasley et al. 1978; Ryde et al. 2002; Tsuji 2009): namely, that the CO fundamental lines cannot be interpreted with a photospheric model only. These lines show an excess absorption (lines with equivalent widths log $W/\nu > -4.75$) that is probably non-photospheric in origin. Figures 1 and 2 clearly show that the central cores of many CO lines cannot be reproduced using a 1D photospheric model in LTE calculation. Tsuji (2008, 2009) proposed instead that the extra-absorption originates from cool molecular layers referred to as a quasi-static molecular dissociation zone; this is sometimes named MOLsphere. Indeed, the formation of these molecular clouds in the outer atmosphere appears to be a basic feature of all red giant stars from early-K to late-M types (see Tsuji 2009, for more details). Therefore, our estimates of the C absolute abundance and of the C and O isotopic ratios are based on a careful selection of the CO lines (i.e., log $W/\nu \leq -4.75$), so that in principle the approximation of LTE synthetic spectra using canonical 1D photospheric models should be valid. By considering this, we derive in Arcturus a C abundance in agreement with that in Ryde et al. (2009). In Aldebaran we derive a C abundance higher by 0.15 dex than the one by Ramírez et al. (2009, see Table 3). On the other hand, the carbon isotopic ratios derived in both stars also agree with previous estimates, it is 9 and 10 for Arcturus and Aldebaran, respectively (see Table 3).

Once the CNO abundances and the C isotopic ratio were estimated, in each star the absorption features caused by ^{17}O and ^{18}O were fitted by the synthetic spectrum varying the abundance of these isotopes to achieve the best fit to each feature, one at a time. We very carefully selected these lines to avoid blending as much as possible, spectral regions where the position of the continuum was regarded as uncertain and/or lines suspected to be affected with weak telluric lines in the rationed spectrum. This resulted in fewer of useful ^{17}O and ^{18}O lines as compared to the study by Harris & Lambert (1984), which was performed

[6] CN lines are very weak in the 5 μm region and cannot be used to derive the N abundance directly.

Table 3. CNO abundances and isotopic ratios.

Star	log ϵ(C)	log ϵ(N)	log ϵ(O)	^{12}C/^{13}C	^{16}O/^{17}O	^{16}O/^{18}O	^{17}O/^{18}O
α Boo	8.06 ± 0.09 (20)	7.67 ± 0.13	8.76 ± 0.17	9 ± 2 (24)	3030 ± 530 (7)	1660 ± 400 (18)	0.55 ± 0.12
α Tau	8.25 ± 0.12 (15)	8.05 ± 0.11	8.48 ± 0.14	10 ± 2 (11)	1670 ± 550 (6)	666 ± 450 (9)	0.4 ± 0.08

Notes. log ϵ(X) = log n_X/n_H + 12, where log n_X is the number density of element X. The number between parenthesis indicates the number of lines used. The N and O abundances are adopted from the literature. We excluded features with both a ^{17}O and ^{18}O contribution (see text).

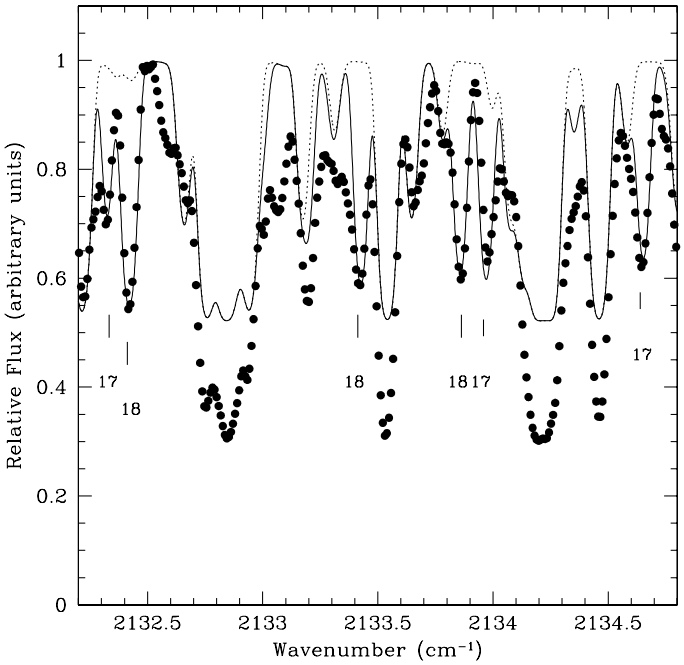

Fig. 2. As Fig. 1 for Aldebaran (filled circles) in another spectral region. Dotted line: ^{12}C/^{13}C = 10 and ^{17}O/^{16}O = ^{18}O/^{16}O = 0; continuous line: the same ^{12}C/^{13}C with ^{17}O/^{16}O = 1670, ^{18}O/^{16}O = 666. Note again the difficulty to fit the cores of the strongest CO lines (see text). Some of the C^{17}O and C^{18}O lines used are marked.

in the same spectral region. However, contrary to these authors, we did not assign any weight to any feature to compute the final O ratios. We also excluded features which both ^{17}O and ^{18}O were contributing. The abundances derived from the various features selected in this way were then combined to give a mean (Table 3).

The main source of uncertainty in deriving the C and O ratios is the dispersion in the ratios obtained from the different lines. Uncertainties caused by errors in the atmospheric parameters (see Table 2) are minor compared to these. As mentioned before, changes in the metallicity of the model atmosphere up to ±0.25 dex have no impact in the derived ratios. The same is true for changes in the N abundance by ±0.3 dex and/or $\Delta T_{\rm eff}$ = ±100 K. Uncertainties in the gravity and microturbulence of the order of those quoted in Table 2 imply errors in the O ratios not exceeding about ±100 in both stars. A stronger impact on the final error comes from the uncertainty in the C and O abundances and the ^{12}C/^{13}C ratio. All these sources of error, once added quadratically, give a total uncertainty of ±180 for Arcturus, and ±230 for Aldebaran. These figures may be safely applied to both O ratios. In Table 3 we indicate the total error in the C and O ratios after including the dispersion in the ratios between different lines. Evidently the dispersion from different lines accounts for most of the total error. Systematic errors may be present, such as the uncertainty in the continuum position and departures from LTE. Owing the weakness of the ^{17}O and ^{18}O lines, errors in the continuum position should affect the ^{17}O and ^{18}O abundances almost equally, so that the ratio ^{17}O/^{18}O is probably more reliable. For the same reason, departures from LTE should be small in the layers where the key features are formed.

When comparing our oxygen ratios with those derived in Harris & Lambert (1984), we agree within the error bars only in the ^{16}O/^{18}O ratio in Aldebaran; we derive considerably higher ^{16}O/^{17}O and ^{17}O/^{18}O ratios in both stars. The differences in the atmosphere parameters adopted ($T_{\rm eff}$, log g, ξ) are not strong enough to explain the discrepancies. Indeed, by using atmosphere models from the Gustafsson et al. (2008) grid with the same stellar parameters and CNO abundances as adopted by Harris & Lambert (1984)[7], we obtain ^{16}O/^{17}O = 2325 and, ^{17}O/^{18}O = 1430 for Arcturus, and ^{16}O/^{17}O = 1540 and ^{17}O/^{18}O = 560 for Aldebaran. The ratios are reduced significantly but not enough (note that we still agree in the ^{16}O/^{18}O ratio in Aldebaran). We recall that Harris & Lambert (1984) used atmosphere models from Bell et al. (1976) and Johnson et al. (1980). The Bell et al. (1976) models are in fact the ancestors of the new grid of spherical MARCS atmosphere models by Gustafsson et al. (2008). These new models considerably improve the atomic and (mainly) molecular opacity treatment, in particular for giant stars, as well as many other physical approximations (see Gustafsson et al. 2008, for a detailed discussion), so that we consider that new MARCS models mimic the real atmospheres of giants much better than the original ones by Bell et al. (1976) and Johnson et al. (1980). An additional source of discrepancy, which is very probably the main cause of our different findings, is the line list used for the CO molecule and the method employed for the continuum placement. First, we note that Harris & Lambert (1984) only included CO lines in their synthetic spectra computations, while we considered several molecular and atomic species (see previous section) in the 4.5 μm spectral region. Indeed, the CO molecule dominates the absorption in this spectral range, but we checked that the remaining molecular species (mainly CN, C_2 and OH) introduce a *veil* of absorption that increases the line intensities and thus affects the isotopic ratios. In particular, the ^{16}O/^{17}O and ^{16}O/^{18}O ratios increase. Secondly, the *gf*-values of the CO lines used by Harris & Lambert (1984) were obtained from Chackerian & Tipping (1983), while here we used those by Goorvitch (1994) on the basis of a more up-to-date electric dipole moment function. As a consequence,

[7] These authors give only the C abundance derived ([C/H] = −0.7 and −0.3, respectively) without any indication of the N and O abundances derived/adopted, nor error bars. Therefore, we scaled the N and O abundances in this test according to the metallicity given in Harris & Lambert (1984) with respect to the solar abundances from Lambert (1978) (we infer that these solar abundances were adopted by these authors; note this circumstance in Figs. 5 and 7 below, where we adopted a conservative error bar of ±0.2 dex in the CNO abundances by Harris & Lambert).

Goortvitch (1994) indeed reported differences up to 3% in the A-values with respect to Chackerian & Tipping (1983) and up to a factor ~6 in the dipole moments in some of the CO isotopes. On the other hand, note that the isotopic lines used are very weak so that the choice of the specific lines might affect the results, in a systematic manner (see above the discussion on the selection of the lines) if there is a systematic difference in the continuum placement. Definitely, the discussion above might explain the differences between the O ratios derived here and those in Harris & Lambert (1984). We believe that our figures are more reliable because they are based on more accurate stellar parameters and CNO abundances, better atmosphere models, and more complete and accurate line lists.

2.4. Physical stellar parameters

To check the reliability of the mass estimates available in the literature (see Table 2), we used the FRANEC code to construct our theoretical Hetzsprung-Russell diagrams. (We warn the reader that the theoretical mass estimate for a single stellar object, obtained by fitting its HR diagram, is quite uncertain. On the other hand, more robust methods, such as the classical isochrones fitting, cannot be applied to our stars.) This was done in the following way. i) First we selected the range of initial masses $M_{\rm ini}$ for which the theoretical HR diagrams could fit the $L, T_{\rm eff}$ values measured and the available estimates for the stellar radii of our stars within their uncertainties. ii) Then, we computed a grid of extra-mixing models over the mass range, looking for the combination of $M_{\rm ini}$ values and transport parameters that allowed the best general fit.

With this procedure, we found it very easy to reproduce the observations for α Tau, assuming initially solar abundance ratios (see Sect. 3); our best estimate for the mass agrees very well with previous determinations. For Arcturus, instead, the procedure were considerably more complex. This is a slightly metal-poor star for which guessing the initial abundance ratios is not straightforward. For C and N we had to rely on the literature, as the measured data are certainly not the initial ones, because they were modified by FDU and extra-mixing. However, there are suggestions that Arcturus belongs to a peculiar *stream* of stars in the vicinity of the Sun; some of them date back to the early seventies (Eggen 1971). Today this stream is considered as being the relic either of an old dissolved cluster (Ramírez & Allende Prieto 2011) or of a captured and disrupted dwarf spheroidal galaxy (Navarro et al. 2004). Its abundances seem to be quite similar to those of the Galactic thick disk, but caution is mandatory. Moreover, there is a considerable dispersion of initial abundances in thick-disc-stars at the metallicity of α Boo, so that we can only put weak constraints on them. The initial values adopted here include a C enhancement by +0.2 dex and an N underabundance by 0.1 dex (Bensby & Feltzing 2006; Matteucci & Chiappini 2003). With these choices, and using an initial enhancement of α-rich elements of +0.4 (including oxygen) from Peterson et al. (1993), the model HR diagrams that can fit the $(L, T_{\rm eff})$ data within the uncertainties correspond to a mass interval from 1 to about 1.25 $M_{\odot}$. The final value we adopted (1.2 $M_{\odot}$) is the only one for which extra-mixing models can reproduce within the errors all the abundance information discussed in Sect. 2.3. The uncertainties on the initial C and N data make our solution less robust than for α Tau, however. Note that our value is slightly higher than that derived by Ramírez & Allende Prieto (2011) (1.08 $M_{\odot}$), who used the Yale code as reference, which has a lower α enhancement.

3. Reproducing the abundances through an extra-mixing model

Whatever the mechanism is that drives non-convective mixing in red giants, Wasserburg et al. (1995) showed that it can be approximated by a circulation occurring at a rate $\dot{M}$, reaching to a maximum temperature T_P, close to, but lower than, the H-burning shell temperature. In a diffusive approach the parameters would instead be the diffusion coefficient D and the total mass involved: the two approaches can be shown to be roughly equivalent (Nollett et al. 2003) in most cases. However, while this is certainly the case when the mixing speed is not relevant (so that the abundance changes depend only on a path integral of reaction rates), it might be different when the velocity of mixing becomes an important issue, diffusive processes are always slow, while other transport mechanisms might not be. Indeed: i) the time available for mixing is not infinite; and ii) the nuclei involved are sometimes unstable with a relatively short half-life: see for example the case of ^{7}Be, decaying into ^{7}Li (Palmerini et al. 2011b). On similar grounds, serious doubts have recently been advanced on some of the proposed mechanisms, such as rotation and thermohaline mixing (Charbonnel & Lagarde 2010; Palmerini et al. 2011b) because of the small diffusion coefficients (or, alternatively, the slow mixing speeds) they can provide, which might make them inadequate to yield the observed abundance changes in the finite time assigned by the duration of the evolutionary stage (Denissenkov & Merryfield 2011).

An important input to the models is the initial CNO admixture of the stellar composition. While for α Tau, a typical thin-disk red giant of relatively high metallicity, we can safely assume solar elemental ratios, for α Boo this is certainly not the case as we already mentioned (see discussion in Sect. 2.4). In our procedure, once the initial CNO abundances are selected, they are employed for choosing the opacity tables to be used. Enhancements in α elements and, to a lesser extent, in C easily introduce substantial changes in the models, from the points of view of both nuclear physics (CNO burning efficiency) and radiative transfer (opacities). We underline this important point because the theoretical HR diagram and the ensuing mass estimate strongly depend on that. Note that using the most recent set of *alpha*-enhanced opacities (see for example Ferguson et al. 2005) theoretical curves are moved to redder regions of the HR diagram than previously found. Therefore, we warn that mass estimates available so far in the literature are actually much more uncertain than currently supposed (see for example Verhoelst et al. 2005; Tsuji 2009; Ramírez & Allende Prieto 2011).

Our best solution implies, for α Tau $M = 1.3\ M_{\odot}$, [Fe/H] = −0.15; for α Boo, $M = 1.2\ M_{\odot}$, [Fe/H] = −0.5, [α/Fe] = 0.4, [C/Fe] = 0.2. As mentioned before, we performed a grid of calculations for both stars: for each choice of the mass allowing a fit (within the uncertainties) to the $L, T_{\rm eff}$ data, we derived the extra-mixing parameters trying to reproduce the chemical abundances; finally, we adopted the case allowing the best compromise in the fit of all available data. There are no ambiguities on α Tau with this procedure, and the resulting HR diagram is shown in Fig. 3.

For α Boo, instead, the solution that we finally adopted appears to require a mass higher than so far assumed and it is strongly dependent on the initial CNO assumed. This point is commented in more detail in Sect. 3.2. The results for the HR diagram and radius of α Boo are displayed in Fig. 4.

According to the above discussion, from the estimate of the mass we derived the time spent on the RGB from the bump in the luminosity function (the small dent in each RGB track indicated by the label "BLF") to the moment in which the observed values

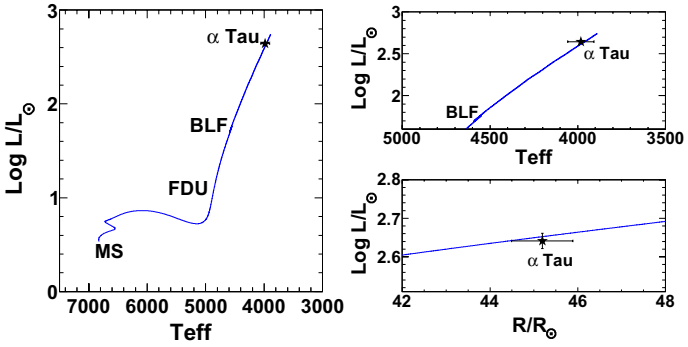

Fig. 3. *Left panel*: a comparison of the observed L and $T_{\rm eff}$ values of α Tau with the adopted evolutionary track in the HR diagram, as derived from the FRANEC code. *Right panel*: zoom of the previous plot (*top*) and a comparison of model and observations for the $L, R_{\rm star}$ relation. The main sequence (MS), first dredge-up (FDU) and BLF positions are marked.

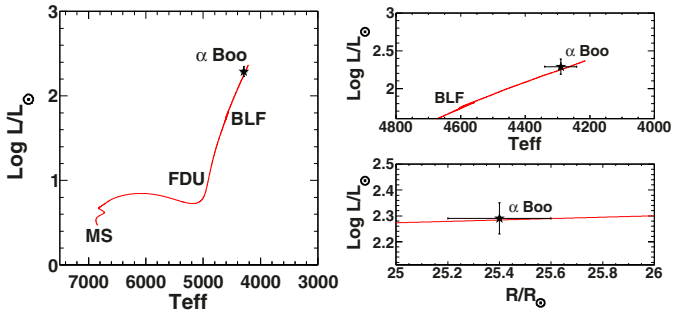

Fig. 4. Same as Fig. 3 for α Boo. Note the peculiar initial CNO content for this star (see text).

of $L, T_{\rm eff}$ are attained. This is the time available for extra-mixing to operate: this is 46 Myr for α Tau and 37 Myr for α Boo. This knowledge allowed us to determine the mixing parameters on observational grounds (albeit with the mentioned cautions for α Boo).

3.1. The technique of the computations

To quantitatively fix the parameters of extra-mixing by using as constraints the observations of α Boo and α Tau discussed so far, we adopted the formalism by Nollett et al. (2003) and calculate the parameters accordingly. After deducing the parameters that allow us to fit the measured abundances, we derived the corresponding mixing speeds needed to achieve the observed abundances in the assigned time. On this basis, we analyzed which of the processes proposed so far in the literature offers a plausible physical mechanism for driving the mixing.

In our procedure we adopted a post-processing code to compute the coupled phenomena of H-burning and transport, taking the detailed stellar parameters from the output of the stellar evolution code (FRANEC: see Cristallo et al. 2011), which provides us with the physical structure of the star.

To describe the nuclear physics phenomena coupled with dynamics one can simply use the total derivatives of stellar abundances:

$$\frac{{\rm d}N_i}{{\rm d}t} = \frac{\partial N_i}{\partial t} + \frac{\partial N_i}{\partial M}\frac{\partial M}{\partial R}\frac{\partial R}{\partial t}, \quad (1)$$

where the partial time derivative due to nucleosynthesis is

$$\frac{\partial N_i}{\partial t} = -N_p N_i \lambda_{i,p} + N_p N_{i-1}\lambda_{i-1,p} - N_i\lambda_{\rm d} + N_{i'}\lambda_{\rm d} \quad (2)$$

and the second term is due to mixing. Here the parameters $\lambda_{i,p}$ are the reaction rates and $\lambda_{\rm d}$ are the decay rates. For the nuclear parameters we adopted the recent upgrades suggested by Adelberger et al. (2011) and Iliadis et al. (2010). Details on our technique for computing extra-mixing and on the descending numerical computations are presented by Palmerini et al. (2011a,b).

3.2. The parametric results

Leaving as free parameters the circulation rate $\dot{M}$ and the temperature T_P of the deepest layers reached by the non-convective mixing, we profited from previous work done for a wide sample of RGB stars by Palmerini et al. (2011a,b) to limit the variation interval of these parameters. Following the formalism used by these authors, the circulation rate was expressed in units of 10^{-6} $M_\odot$/yr, through the parameter $\dot{M}_6$. The temperature of the deepest layers attained by the mass transport, T_P, was considered through the parameter $\Delta = \log T_{\rm H} - \log T_P$, where $T_{\rm H}$ is the temperature at which the maximum energy from H burning in the shell is released. Although this is certainly a not-very-intuitive way of expressing the mixing depth, it offers a sort of rule-of-thumb criterion, established by Nollett et al. (2003). If Δ is lower than about 0.1, post-process mixing models are quite safe in the sense that any nucleosynthesis occurring during the transport will not add significant energy to the stellar budget, and consequently will not alter the reference stellar structure.

On this basis $\dot{M}_6$ was allowed to vary in the range from 0.01 to 0.3 and Δ in the range from 0.18 to 0.22. For each combination of values of the two parameters we computed the corresponding post-process mixing models, starting from the stellar structure along the RGB as provided by full calculations (with no extra-mixing) made with the FRANEC code. The technique adopted is that of reading the physical parameters at and above the H burning shell from the outputs of the stellar code up to the convective envelope using them to compute the outcomes of the coupled processes of burning and mixing with the parameters adopted; the inputs from the full model stellar structure are periodically refreshed, to ensure a maintained coherence between the extra-mixing calculations and the real physics of the star.

Among the many runs performed we show in Table 4 i) those computed for α Tau, using our best choice for its mass; and ii) those computed for α Boo, using our mass estimate (1.2 $M_\odot$) and iii) those run by adopting the mass values given by Ramírez & Allende Prieto (2011).

The comparison of model sequences for isotopic and elemental abundances with observed data is presented in Figs. 5 to 8 for the best cases selected from Table 4. Here the curves with different line types refer to different choices of the parameters, according to the explainations in the labels.

In particular, Fig. 5 shows the evolution of the ^{12}C/^{13}C ratio and of the elemental CNO abundances along the RGB for extra-mixing models adopted for α Tau as a function of the effective temperature (which in this case is a proxy for time, as red giants become progressively redder and cooler when they evolve). The label BLF identifies the abundances as determined by the FDU (these are the same as those characterizing the envelope layers at the bump of the luminosity function). Clearly, there is no way of explaining the carbon isotopic ratio with a model that does not invoke extra-mixing. This indeed (dotted curve) presents a

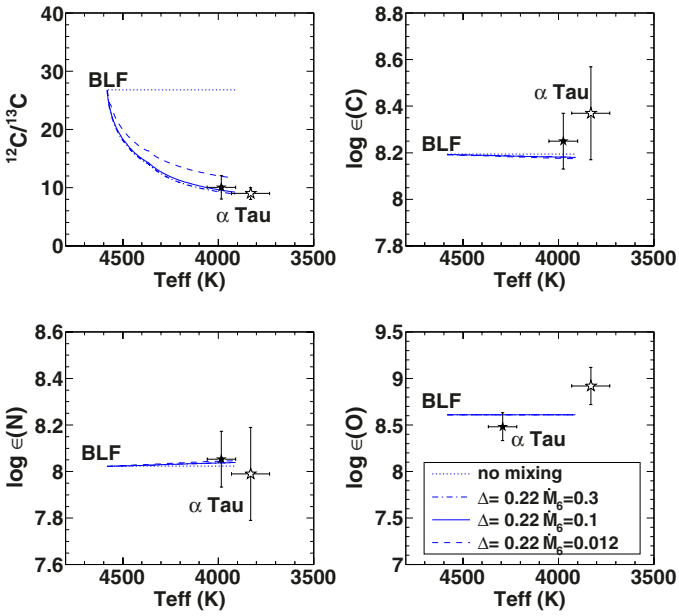

Fig. 5. Evolution of the $^{12}C/^{13}C$ ratio and of the elemental CNO abundances as a function of the model effective temperature in selected extra-mixing runs performed for α Tau compared to observed data. Black stars show the observational data presented in this work, while open stars report abundances from Harris & Lambert (1984). A case without extra-mixing is reported for comparison (dotted line). See text for details.

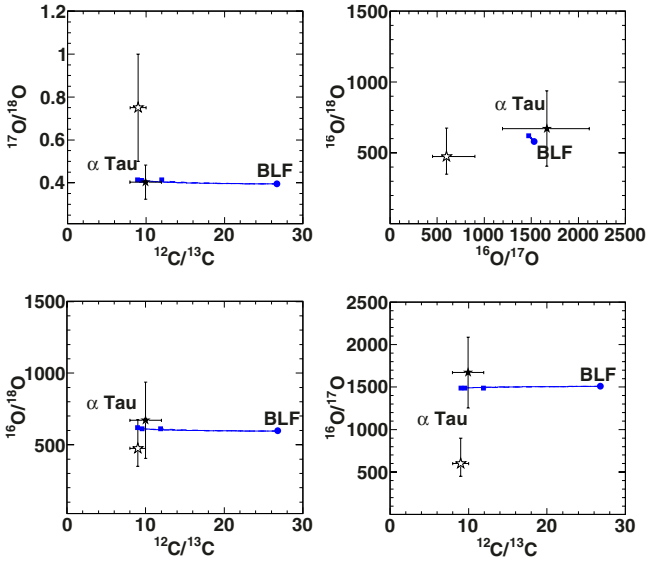

Fig. 6. Combinations of isotopic C and O ratios for selected extra-mixing runs performed for α Tau and for a case without extra-mixing (blue spot) compared to observed data. The models and the meaning of the line types are the same as in Fig. 5. The small squares indicate the envelope isotopic mix reached by each mixing case when the model effective temperature is comparable with the observed one. At the same mixing depth, the higher the mixing rate $\dot{M}_6$, the lower the value of the carbon isotopic ratio. Open stars are the isotopic ratios derived by Harris & Lambert (1984).

$^{12}C/^{13}C$ ratio compared to the observations that is too high. The same conclusion can be obtained by an inspection of Fig. 6, where the model combinations of the C and O isotopic ratios are compared with the observations. In this plot the case without extra-mixing is represented by a single dot, since neither carbon nor oxygen change their isotopic ratios along the RGB. An extra-mixing model with an excessively penetration (those with $\Delta = 0.18$) can be excluded on the basis of its high $^{17}O/^{18}O$ ratios and of its low absolute carbon abundance (see Table 4). A case with an intermediate depth ($\Delta = 0.20$) would alleviate the problem of oxygen isotopic ratios, but would still predict insufficiently carbon abundance. Therefore a fairly shallow extra-mixing is needed ($\Delta = 0.22$) for α Tau. Concerning its efficiency in terms of mass circulation, all the cases lie within the observed range, apart from that with the lowest efficiency ($\dot{M}_6 = 0.01$). The $\dot{M}_6 = 0.012$ case shows the maximum allowed $^{12}C/^{13}C$ ratio, while extra-mixing models in the range $0.03 \leq \dot{M}_6 \leq 0.3$ reproduce all observed constraints well. We recall again that the most critical point is certainly the $^{12}C/^{13}C$ ratio, even if oxygen isotopic ratios help in constraining the extra-mixing depth. The choice of the parameters found to be appropriate agrees well with the cases run by Palmerini et al. (2011a,b), so that α Tau appears to be really a typical template for Population I red giants, also regarding the mixing processes.

Figures 7 and 8 integrate the previous picture by showing the more complex case of α Boo. As discussed previously, here the constraints from elemental abundances are quite weak, depending on assumptions made for their unknown initial CNO values. Despite this caution, it is noticeable that the extra-mixing parameters determined for α Tau ($0.03 \leq \dot{M}_6 \leq 0.3$, $\Delta = 0.22$) also reproduce the constraints for α Boo well. This is, in our opinion, a very interesting finding, because the two red giants have a different metallicity. Many of the computed cases have been

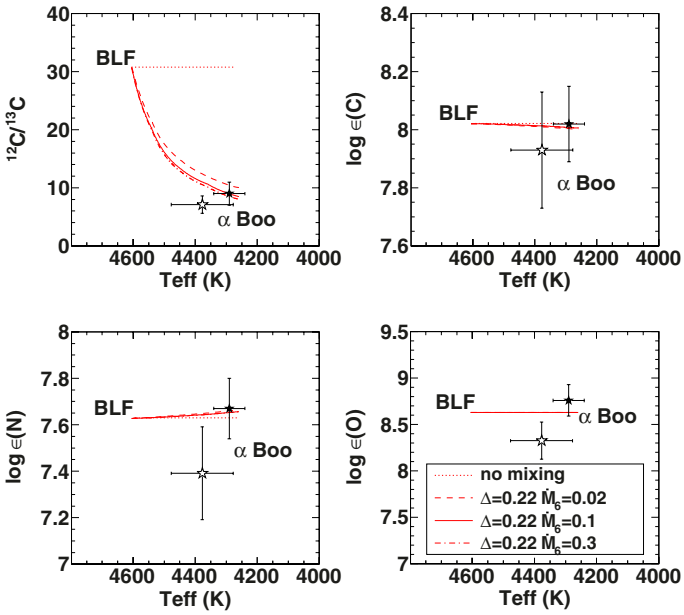

Fig. 7. Same as Fig. 5 for α Boo.

excluded on the basis of reasonings similar to those exposed for α Tau (see Table 4). Considering the full extension of the error bars for the observations, extra-mixing cases with a rather slow circulation ($0.01 \leq \dot{M}_6 \leq 0.03$) cannot be a priori excluded for α Boo. Notwithstanding, the global quality of the fits is much better with higher $\dot{M}_6$ values, i.e., with a choice similar to that for α Tau.

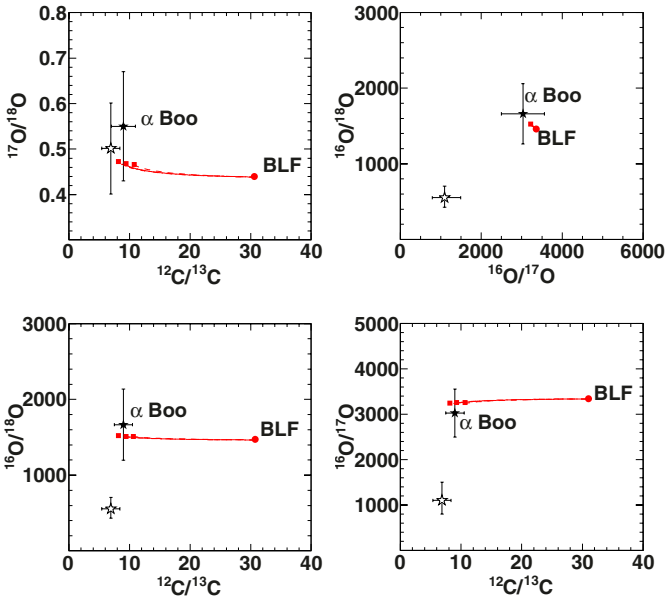

Fig. 8. Same as Fig. 6 for α Boo.

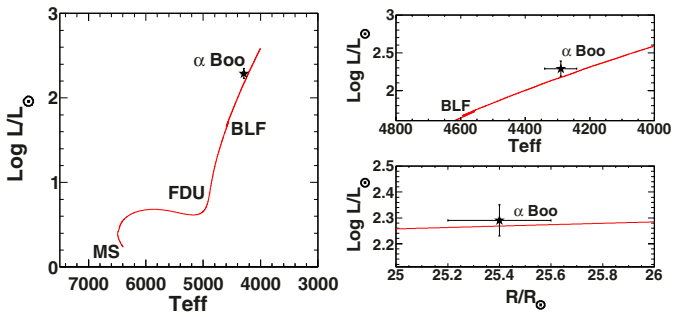

Fig. 9. Same as Fig. 4, but with a choice of 1.08 $M_\odot$ (see text for details).

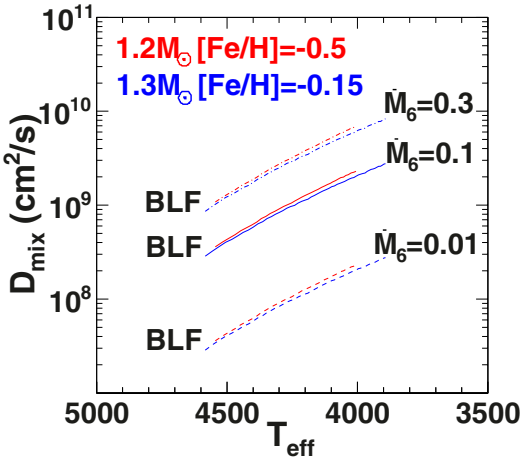

Fig. 10. Diffusion coefficients approximating our circulation models assuming a diffusive treatment (see text for details). The parameters of the considered cases are shown in the labels.

From a more detailed inspection of Table 4 it emerges that, as far as the abundances are concerned, adopting a slightly lower mass than found by us (for example for 1.08 $M_\odot$, the value determined by Ramírez & Allende Prieto 2011) several (albeit not all) data can be reproduced with a different choice of the parameters ($\Delta \sim 0.18$, $\dot{M}_6 \sim 0.015$), that is, with a slightly deeper and slower extra-mixing. Remarkable discrepancies emerge in this case only for the absolute elemental abundances, whose modeling suffers for the uncertainties in the initial composition already discussed. However, for $M = 1.08\ M_\odot$ a poorer fit to the luminosity and radius of α Boo is obtained (see Fig. 9). We therefore maintain our previous choice of the mass (1.2 $M_\odot$) as our best case, but we remark that it, too, is rather uncertain.

4. Discussion and conclusions

We notice that the values of the extra-mixing parameters deduced for our stars nicely fit with those previously found to be typical for red giants of Population I, from their CNO isotopic and elemental abundance ratios as well as from their Li content (Palmerini et al. 2011a,b). Under these premises, we are tempted to conclude that extra-mixing during the RGB phase presents common properties for solar or moderately low metallicities. The idea is suggestive, although we cannot draw too firm conclusions at this level. A wider sample of moderately metal-poor, well-measured red giants, permitting reliable statistics (like that selected by Palmerini et al. 2011a, for higher metallicities) would be required for this.

It is relevant to compare our findings to those proposed in the literature, adopting the complementary view of a diffusive approach. In particular, Denissenkov (2010) and Denissenkov & Merryfield (2011) recently performed 1D studies of the effects of thermohaline diffusion (which can be easily compared to our discussion) and then substantiated their results with 2D- and 3D-simulations. In Denissenkov (2010) it was shown that thermohaline mixing might guarantee diffusion coefficients $D_{\rm mix}$ lower than a few 10^6 cm^2/s (see especially their Fig. 3, in which $D_{\rm mix}$ was normalized to the the thermal diffusivity. This last was assumed to be about 10^8, as specified in Table 1 of that paper). However, in the subsequent discussion (in particular from Figs. 7, 11, and 12) the author clarified that, to fit all the red giant data (including the values of C/Fe and the isotopic ratios $^{12}C/^{13}C$ lower than about 15) one would need much higher values of $D_{\rm mix}$. These last seem to be compatible with thermohaline mixing only for low metallicities, however. In our case we can make a rough estimate of $D_{\rm mix}$ from the simplified correspondence between the circulation and diffusion treatments established by Nollett et al. (2003), i.e., $D_{\rm equiv} \simeq (l \times \dot{M})/4\pi\rho r^2$.

For $\dot{M} = (0.3\text{–}3) \times 10^{-7}\ M_\odot$/yr (the range found to be good for our stars) and adopting the values of the other parameters from the stellar code outputs, we obtain values of $D_{\rm equiv}$ as those plotted in Fig. 10 (see also the last column in Table 4 where average $D_{\rm equiv}$ values of each extra-mixing case are reported). For the acceptable cases they cover a range centered around a few 10^9 cm^2/s (this last value being roughly the average).

We can compare this with the data of Fig. 12 in Denissenkov (2010), where the curve for $D_{\rm mix}$ providing the best fit to the data is plotted as a function of the radius. The radius of the convective envelope border in α Tau, in the phases after the BLF, spans the range $\log[r/R_\odot] = -0.13$ to -0.07. For these values the average value $D_{\rm mix}$ is again 10^9 cm^2/s, in agreement with the value found by us. Hence, with a completely independent treatment, we confirm the results of this paper. The diffusion coefficient required for explaining the observations of α Tau (and the more uncertain

α Boo) must be quite high (such a value for $D_{\rm mix}$ implies in our cases a velocity of a few hundredths cm/s).

Note that also the treatment by Palmerini et al. (2011a), favoring $\dot{M}$ values very similar to those of α Tau and α Boo, would provide the same consequences for the values of $D_{\rm mix}$.

By pursuing a similar discussion in the framework of multi-D models of the radiative zones, Denissenkov & Merryfield (2011) showed that this is related to aspect ratios (length over diameter) of the dynamical instabilities generated in the simulations: with thermohaline mixing these aspect ratios would be too low, i.e., the unstable blobs would be too similar to "bubbles" instead of the required "finger"-like structures.

Whatever approach is used, the results seem to converge in saying that pure thermohaline diffusion might have difficulties in explaining the observed abundances of high-metallicity red giants, at least when it is taken alone; the possibility of a modified magneto-thermohaline mixing was envisaged by Denissenkov et al. (2009) but is not yet substantiated by detailed models. When the results by Charbonnel & Lagarde (2010) are considered one sees that any diffusion induced by rotational effects is in its turn insufficient; in this case D is too small by several orders of magnitude (see Fig. 9 in that paper).

We have to notice that in some recent works (see for example Angelou et al. 2011) the authors wisely avoid the use of the term "thermohaline diffusion" to indicate chemical readjustments started by a molecular weight inversion; they prefer the name $\Delta\mu$ *mixing*. The use of the term diffusion could have remarkable implications. Indeed, while diffusion is intrinsically a slow phenomenon and thermal diffusion should be slow, it is not guaranteed that the μ gradient inversion, the chemicals would diffuse with a speed comparable to that of heat. We have no elements at this stage to exclude that non-diffusive mixing of a suitable velocity might occur as a consequence of a "$\Delta\mu$" effect: in that case, it would offer a realistic mechanism. Our analysis only underlines that very slow mixing, as in diffusive processes, would be inadequate to explain the chemical abundances; but there is clearly much that we still have to learn about the real physical processes.

One has to underline that magnetic buoyancy, recently advocated in various ways by Busso et al. (2007); Nordhaus et al. (2008); Denissenkov et al. (2009) is suitable to provide the mixing velocities (or the $D_{\rm mix}$ values) we require for the examined stars. Recalling old, seminal works by Parker (for example Parker 1974) one sees that the velocity of buoyant magnetic structures, in presence of thermal exchanges with the environment, is roughly $v = K/a^2$, where a is a typical linear dimension of the rising bubbles. Using parameters suitable for evolved red giants (Parker instead analyzed the Sun), K turns out to be of about 10^{13}–10^{14} (cgs units). Hence, large structures (100–1000 km-size) would travel at moderate speeds, about the velocity required on the RGB, while small instabilities (1 km-size) would provide the situation envisaged for the AGB phases in Busso et al. (2007), with high speed, close to the Alfvén velocity. All cases in between these extremes are possible. If this is the real physical situation (which still has to be proven on the basis of MHD simulations), then our results would suggest that on the RGB large magnetic domains, moving at moderate speed, are involved in the buoyancy.

Recently (Drake et al. 2011), the association between non-convective mixing and magnetic activity seems to have been demonstrated nicely for the bright, very active RS CVn-type variable λ And (see for example Andrews et al. 1988). This star shows CNO anomalies well before reaching the BLF. This finding, and the fact that one of our stars (α Boo) is known to have both a chromosphere (Ayres & Linsky 1975) and indications of photospheric magnetic fields from the Zeeman effect (Sennhauser & Berdyugina 2011), seem indeed to suggest magnetic mechanisms as very promising physical causes for driving extra-mixing in red giants.

Acknowledgements. Part of this work was supported by the Spanish grant AYA2011-22460. S.C. acknowledges financial support from Italian Grant FIRB 2008 "FUTURO IN RICERCA" C81J10000020001 and from PRIN-INAF 2011 "Multiple populations in Globular Clusters: their role in the Galaxy assembly". The authors would like to thank to K. Hinkle for providing the infrared spectra of Aldebaran (α Tau). We are grateful to the refereee for very pertinent and useful suggestions.

References

Adelberger, E. G., García, A., Robertson, R. G. H., et al. 2011, Rev. Mod. Phys., 83, 195
Alvarez, R., & Plez, B. 1998, A&A, 330, 1109
Alves-Brito, A., Meléndez, J., Asplund, M., Ramírez, I., & Yong, D. 2010, A&A, 513, A35
Amari, S., Nittler, L. R., Zinner, E., Lodders, K., & Lewis, R. S. 2001, ApJ, 559, 463
Andrews, A. D., Rodono, M., Linsky, J. L., et al. 1988, A&A, 204, 177
Angelou, G. C., Church, R. P., Stancliffe, R. J., Lattanzio, J. C., & Smith, G. H. 2011, ApJ, 728, 79
Asplund, M., Grevesse, N., Sauval, A. J., & Scott, P. 2009, ARA&A, 47, 481
Ayres, T. R., & Linsky, J. L. 1975, ApJ, 200, 660
Barber, R. J., Tennyson, J., Harris, G. J., & Tolchenov, R. N. 2006, MNRAS, 368, 1087
Bell, R. A., Eriksson, K., Gustafsson, B., & Nordlund, A. 1976, A&AS, 23, 37
Bensby, T., & Feltzing, S. 2006, MNRAS, 367, 1181
Brown, J. A., & Wallerstein, G. 1989, AJ, 98, 1643
Busso, M., Wasserburg, G. J., Nollett, K. M., & Calandra, A. 2007, ApJ, 671, 802
Cami, J., Sloan, G. C., Markwick-Kemper, A. J., et al. 2009, ApJ, 690, L122
Chackerian, Jr., C., & Tipping, R. H. 1983, J. Mol. Spectr., 99, 431
Charbonnel, C. 2004, Origin and Evolution of the Elements, 59
Charbonnel, C., & Balachandran, S. C. 2000, A&A, 359, 563
Charbonnel, C., & Lagarde, N. 2010, A&A, 522, A10
Charbonnel, C., & Zahn, J.-P. 2007, A&A, 467, L15
Cristallo, S., Straniero, O., Gallino, R., et al. 2009, ApJ, 696, 797
Cristallo, S., Piersanti, L., Straniero, O., et al. 2011, ApJS, 197, 17
Denissenkov, P. A. 2010, ApJ, 723, 563
Denissenkov, P. A., & Merryfield, W. J. 2011, ApJ, 727, L8
Denissenkov, P. A., & Tout, C. A. 2003, MNRAS, 340, 722
Denissenkov, P. A., Da Costa, G. S., Norris, J. E., & Weiss, A. 1998, A&A, 333, 926
Denissenkov, P. A., Pinsonneault, M., & MacGregor, K. B. 2009, ApJ, 696, 1823
Drake, J. J., Ball, B., Eldridge, J. J., Ness, J.-U., & Stancliffe, R. J. 2011, AJ, 142, 144
Eggen, O. J. 1971, PASP, 83, 271
Eggleton, P. P., Dearborn, D. S. P., & Lattanzio, J. C. 2006, Science, 314, 1580
Ferguson, J. W., Alexander, D. R., Allard, F., et al. 2005, ApJ, 623, 585
Goldman, A., Schoenfeld, W. G., Goorvitch, D., et al. 1998, J. Quant. Spec. Radiat. Transf., 59, 453
Goorvitch, D. 1994, ApJS, 95, 535
Gratton, R. G., Sneden, C., Carretta, E., & Bragaglia, A. 2000, A&A, 354, 169
Grundahl, F., Briley, M., Nissen, P. E., & Feltzing, S. 2002, A&A, 385, L14
Gustafsson, B., Edvardsson, B., Eriksson, K., et al. 2008, A&A, 486, 951
Harris, M. J., & Lambert, D. L. 1984, ApJ, 285, 674
Hase, F., Wallace, L., McLeod, S. D., Harrison, J. J., & Bernath, P. F. 2010, J. Quant. Spec. Radiat. Transf., 111, 521
Heasley, J. N., Ridgway, S. T., Carbon, D. F., Milkey, R. W., & Hall, D. N. B. 1978, ApJ, 219, 970
Hinkle, K. H., Lambert, D. L., & Snell, R. L. 1976, ApJ, 210, 684
Hinkle, K., Wallace, L., & Livingston, W. 1995, PASP, 107, 1042
Iliadis, C., Longland, R., Champagne, A. E., Coc, A., & Fitzgerald, R. 2010, Nucl. Phys. A, 841, 31
Johnson, H. R., Bernat, A. P., & Krupp, B. M. 1980, ApJS, 42, 501
Kupka, F. G., Ryabchikova, T. A., Piskunov, N. E., Stempels, H. C., & Weiss, W. W. 2000, Baltic Astron., 9, 590
La Cognata, M., Spitaleri, C., Mukhamedzhanov, A., et al. 2010, ApJ, 708, 796
Lambert, D. L. 1978, MNRAS, 182, 249

Langhoff, S. R., & Bauschlicher, Jr., C. W. 1993, Chem. Phys. Lett., 211, 305
Lebzelter, T., Heike, U., Abia, C., et al. 2012, A&A, in press
Matteucci, F., & Chiappini, C. 2003, in ASP Conf. Ser. 304, eds. C. Charbonnel, D. Schaerer, & G. Meynet, 384
Navarro, J. F., Helmi, A., & Freeman, K. C. 2004, ApJ, 601, L43
Nicolussi, G. K., Davis, A. M., Pellin, M. J., et al. 1997, Science, 277, 1281
Nicolussi, G. K., Pellin, M. J., Lewis, R. S., et al. 1998, Phys. Rev. Lett., 81, 3583
Nittler, L. R., Alexander, C. M. O., Gao, X., Walker, R. M., & Zinner, E. 1997, ApJ, 483, 475
Nittler, L. R., Alexander, C. M. O., Gallino, R., et al. 2008, ApJ, 682, 1450
Nollett, K. M., Busso, M., & Wasserburg, G. J. 2003, ApJ, 582, 1036
Nordhaus, J., Busso, M., Wasserburg, G. J., Blackman, E. G., & Palmerini, S. 2008, ApJ, 684, L29
Palmerini, S., Cristallo, S., Busso, M., et al. 2011a, ApJ, 741, 26
Palmerini, S., La Cognata, M., Cristallo, S., & Busso, M. 2011b, ApJ, 729, 3
Parker, E. N. 1974, Ap&SS, 31, 261
Peterson, R. C., Dalle Ore, C. M., & Kurucz, R. L. 1993, ApJ, 404, 333
Querci, F., Querci, M., & Kunde, V. G. 1971, A&A, 15, 256
Ram, R. S., Wallace, L., & Bernath, P. F. 2010a, J. Mol. Spectr., 263, 82
Ram, R. S., Wallace, L., Hinkle, K., & Bernath, P. F. 2010b, ApJS, 188, 500
Ramírez, I., & Allende Prieto, C. 2011, ApJ, 743, 135
Ramírez, I., Meléndez, J., & Asplund, M. 2009, A&A, 508, L17
Rothman, L. S., & Gordon, I. E. 2009, in 64th International Symposium On Molecular Spectroscopy
Ryde, N., Lambert, D. L., Richter, M. J., & Lacy, J. H. 2002, ApJ, 580, 447
Ryde, N., Edvardsson, B., Gustafsson, B., et al. 2009, A&A, 496, 701
Sennhauser, C., & Berdyugina, S. V. 2011, in ASP Conf. Ser. 448, eds. C. Johns-Krull, M. K. Browning, & A. A. West, 1255
Skory, S., Weck, P. F., Stancil, P. C., & Kirby, K. 2003, ApJS, 148, 599
Smith, V. V., & Lambert, D. L. 1990, ApJS, 72, 387
Soubiran, C., Le Campion, J.-F., Cayrel de Strobel, G., & Caillo, A. 2010, A&A, 515, A111
Talon, S. 2005, in EAS Publ. Ser. 17, eds. G. Alecian, O. Richard, & S. Vauclair, 187
Tomkin, J., & Lambert, D. L. 1984, ApJ, 279, 220
Tsuji, T. 2008, A&A, 489, 1271
Tsuji, T. 2009, A&A, 504, 543
Ulrich, R. K. 1971, ApJ, 168, 57
Uttenthaler, S., Lebzelter, T., Palmerini, S., et al. 2007, A&A, 471, L41
Verhoelst, T., Bordé, P. J., Perrin, G., et al. 2005, A&A, 435, 289
Wasserburg, G. J., Boothroyd, A. I., & Sackmann, I. 1995, ApJ, 447, L37
Weiss, A., Denissenkov, P. A., & Charbonnel, C. 2000, A&A, 356, 181
Zahn, J.-P. 1992, A&A, 265, 115

Page 12 is available in the electronic edition of the journal at http://www.aanda.org

Table 4. CNO abundances, C and O isotopic ratios and equivalent diffusive coefficients for the calculated extra-mixing models.

		log ϵ(C)	log ϵ(N)	log ϵ(O)	^{12}C/^{13}C	^{16}O/^{17}O	^{16}O/^{18}O	^{17}O/^{18}O	$D_{\rm equiv}$ (cm^2 s^{-1})
α Tau (obs)		8.25 ± 0.12	8.05	8.48	10 ± 2	1670 ± 550	666 ± 450	0.4 ± 0.08	
FDU	$M_\odot$ = 1.3	8.18	8.02	8.61	26.76	1508	595	0.39	
Δ = 0.22	$\dot{M}_6$ = 0.01	8.14	8.05	8.61	12.52	1489	611	0.41	1.14×10^8
Δ = 0.22	$\dot{M}_6$ = 0.012	8.14	8.04	8.61	11.96	1489	611	0.41	1.37×10^8
Δ = 0.22	$\dot{M}_6$ = 0.015	8.14	8.04	8.61	11.53	1490	611	0.41	1.71×10^8
Δ = 0.22	$\dot{M}_6$ = 0.03	8.14	8.04	8.61	10.34	1490	611	0.41	3.42×10^8
Δ = 0.22	$\dot{M}_6$ = 0.1	8.14	8.04	8.61	9.56	1490	612	0.41	1.15×10^9
Δ = 0.22	$\dot{M}_6$ = 0.3	8.14	8.04	8.61	9.22	1489	612	0.41	3.45×10^9
Δ = 0.2	$\dot{M}_6$ = 0.01	8.1	8.08	8.61	11.42	1459	636	0.44	1.15×10^8
Δ = 0.2	$\dot{M}_6$ = 0.015	8.1	8.08	8.61	9.22	1458	639	0.44	1.73×10^8
Δ = 0.2	$\dot{M}_6$ = 0.03	8.09	8.08	8.61	7.23	1459	640	0.44	3.45×10^8
Δ = 0.2	$\dot{M}_6$ = 0.1	8.09	8.07	8.61	6.07	1459	641	0.44	1.15×10^9
Δ = 0.2	$\dot{M}_6$ = 0.3	8.09	8.07	8.61	5.76	1459	641	0.44	3.45×10^9
Δ = 0.18	$\dot{M}_6$ = 0.01	8.05	8.14	8.61	14.16	1383	694	0.5	1.15×10^8
Δ = 0.18	$\dot{M}_6$ = 0.015	8.05	8.14	8.61	14.16	1383	694	0.5	1.73×10^8
Δ = 0.18	$\dot{M}_6$ = 0.03	7.99	8.16	8.61	5.94	1378	721	0.52	3.45×10^8
Δ = 0.18	$\dot{M}_6$ = 0.1	7.97	8.16	8.61	4.14	1380	728	0.53	1.15×10^9
Δ = 0.18	$\dot{M}_6$ = 0.3	7.96	8.16	8.61	3.78	1380	731	0.53	3.45×10^9
α Boo (obs)		8.06 ± 0.09	7.67	8.76	9 ± 2	3030 ± 530	1660 ± 400	0.55 ± 0.12	
FDU	$M_\odot$ = 1.2	8.01	7.73	8.63	30.74	3341	1465	0.44	
Δ = 0.22	$\dot{M}_6$ = 0.01	7.97	7.76	8.63	13.14	3248	1506	0.46	6.84×10^7
Δ = 0.22	$\dot{M}_6$ = 0.015	7.97	7.76	8.63	11.64	3248	1507	0.46	1.03×10^8
Δ = 0.22	$\dot{M}_6$ = 0.02	7.97	7.76	8.63	10.85	3235	1511	0.47	1.37×10^8
Δ = 0.22	$\dot{M}_6$ = 0.03	7.97	7.75	8.63	10.41	3249	1507	0.46	2.05×10^8
Δ = 0.22	$\dot{M}_6$ = 0.1	7.97	7.75	8.63	9.42	3248	1508	0.46	6.84×10^8
Δ = 0.22	$\dot{M}_6$ = 0.3	7.96	7.75	8.63	8.94	3244	1511	0.47	2.05×10^9
Δ = 0.2	$\dot{M}_6$ = 0.01	7.93	7.82	8.63	12.5	3081	1580	0.51	6.86×10^7
Δ = 0.2	$\dot{M}_6$ = 0.015	7.92	7.81	8.63	9.46	3089	1581	0.51	1.03×10^8
Δ = 0.2	$\dot{M}_6$ = 0.03	7.92	7.81	8.63	7.28	3099	1581	0.51	2.06×10^8
Δ = 0.2	$\dot{M}_6$ = 0.1	7.91	7.8	8.63	5.81	3093	1588	0.51	6.86×10^9
Δ = 0.2	$\dot{M}_6$ = 0.3	7.91	7.8	8.63	5.48	3094	1588	0.51	2.06×10^9
Δ = 0.18	$\dot{M}_6$ = 0.01	7.88	7.89	8.63	17.56	2718	1736	0.64	6.89×10^7
Δ = 0.18	$\dot{M}_6$ = 0.015	7.84	7.91	8.63	11.2	2681	1788	0.67	1.03×10^8
Δ = 0.18	$\dot{M}_6$ = 0.03	7.8	7.92	8.63	6.21	2685	1827	0.68	2.07×10^8
Δ = 0.18	$\dot{M}_6$ = 0.1	7.76	7.93	8.63	3.94	2684	1863	0.69	6.89×10^8
Δ = 0.18	$\dot{M}_6$ = 0.3	7.75	7.94	8.63	3.54	2684	1874	0.7	2.07×10^9
α Boo (obs)		8.06 ± 0.09	7.67	8.76	9 ± 2	3030 ± 530	1660 ± 400	0.55 ± 0.12	
FDU	$M_\odot$ = 1.08	8.03	7.67	8.63	32.72	5204	1393	0.27	
Δ = 0.22	$\dot{M}_6$ = 0.01	7.97	7.74	8.63	10.23	4834	1461	0.3	6.27×10^7
Δ = 0.22	$\dot{M}_6$ = 0.015	7.97	7.74	8.63	8.73	4819	1465	0.3	9.41×10^7
Δ = 0.22	$\dot{M}_6$ = 0.03	7.96	7.74	8.63	7.53	4813	1467	0.3	1.88×10^8
Δ = 0.22	$\dot{M}_6$ = 0.1	7.96	7.73	8.63	6.84	4817	1467	0.3	6.27×10^8
Δ = 0.22	$\dot{M}_6$ = 0.3	7.96	7.73	8.63	6.61	4815	1468	0.3	1.88×10^9
Δ = 0.2	$\dot{M}_6$ = 0.01	7.9	7.83	8.63	9.8	4246	1582	0.37	6.29×10^7
Δ = 0.2	$\dot{M}_6$ = 0.015	7.89	7.85	8.63	7.17	4219	1599	0.38	9.44×10^7
Δ = 0.2	$\dot{M}_6$ = 0.03	7.87	7.84	8.63	5.27	4218	1610	0.38	1.89×10^8
Δ = 0.2	$\dot{M}_6$ = 0.1	7.86	7.84	8.63	4.27	4221	1617	0.38	6.29×10^8
Δ = 0.2	$\dot{M}_6$ = 0.3	7.85	7.84	8.63	4.03	4213	1622	0.38	1.89×10^9
Δ = 0.18	$\dot{M}_6$ = 0.01	7.83	7.93	8.63	14.33	3103	1859	0.6	6.31×10^7
Δ = 0.18	$\dot{M}_6$ = 0.015	7.78	7.95	8.63	8.34	3232	1902	0.59	9.47×10^7
Δ = 0.18	$\dot{M}_6$ = 0.03	7.69	7.99	8.63	4.88	2986	2102	0.7	1.89×10^8
Δ = 0.18	$\dot{M}_6$ = 0.1	7.59	8.03	8.63	3.27	2917	2264	0.78	6.31×10^8
Δ = 0.18	$\dot{M}_6$ = 0.3	7.57	8.04	8.63	3.04	2945	2283	0.78	1.89×10^9